Supplementary information to

Predicting the Near Field Underwater Explosion Response of Coated Composite Cylinders using Multiscale Simulations, Experiments, and Machine Learning

Sumeru Nayak[1], Gideon A. Lyngdoh[1], Arun Shukla[2], and Sumanta Das[3*]

[1] Graduate Student, Civil and Environmental Engineering, University of Rhode Island, Kingston, RI, USA

[2] Simon Ostrach Professor, Mechanical, Industrial and Systems Engineering, University of Rhode Island, Kingston, RI, USA

[3*]Assistant Professor, Civil and Environmental Engineering, University of Rhode Island, Kingston, RI 02881, USA, Email: sumanta_das@uri.edu (corresponding author)

This supplementary material elaborates certain contents of the manuscript for enhanced readability and ease of reference. The codes for the same are available in https://github.com/iamsumeru/MultiDataGen.git. Section A provides the iterative stress update algorithms for the micro and meso scales. Section B elaborates and lists the material properties used in various scales of the simulations. While Section B-1 lists the matrix, fiber, and matrix-fiber interfacial behavior in the micro-scale, Section B-2 lists additional interface properties required for mesoscale analyses. Section B-3 lists additional interlaminar behavior and coating polymers' rate-dependent behavior. Section C elucidates the choice of element size and mesh convergence in the multiscale simulations. Section D shows some additional features of the developed numerical framework that can be implemented to extend the capabilities of the multiscale framework facilitating potential design strategies for thick laminates. Section E shows the correlation between additional DIC plots observed experimentally and the simulated responses. The optimized neural network is provided in Section F.

A. Iterative Stress Update Approach at Micro and Meso Scales

The computational strategy adopted in the study follows an iterative framework. Figure A.1 shows the steps for micro-scale analysis while Figure A.2 shows the steps for meso-scale analysis.

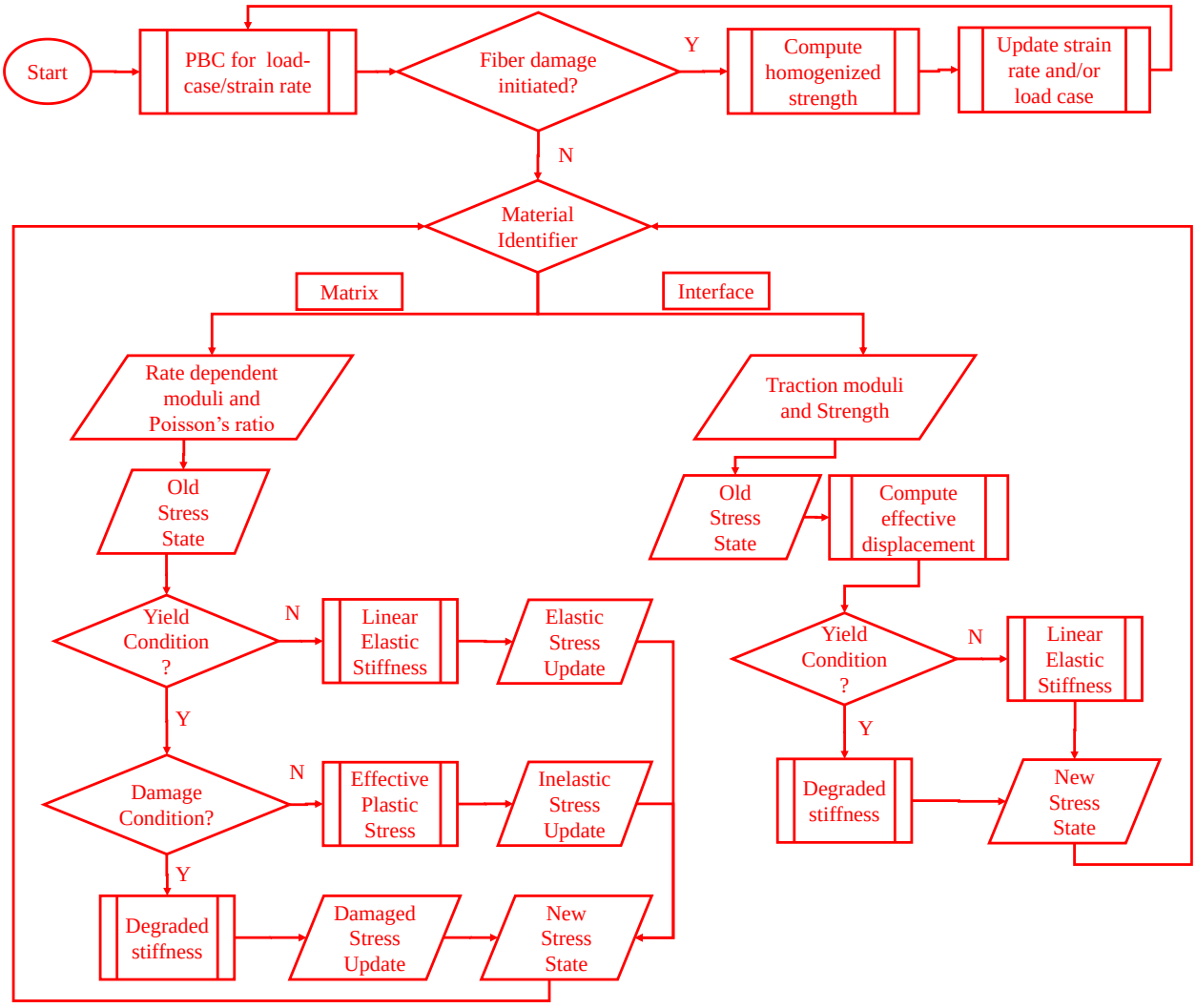

Figure A.1. Steps for computing homogenized response of micro-scale unit cell

The homogenized response from the micro-scale is used as inputs to the meso-scale. Figure A.2 shows the stress update algorithm for the meso-scale unit cell.

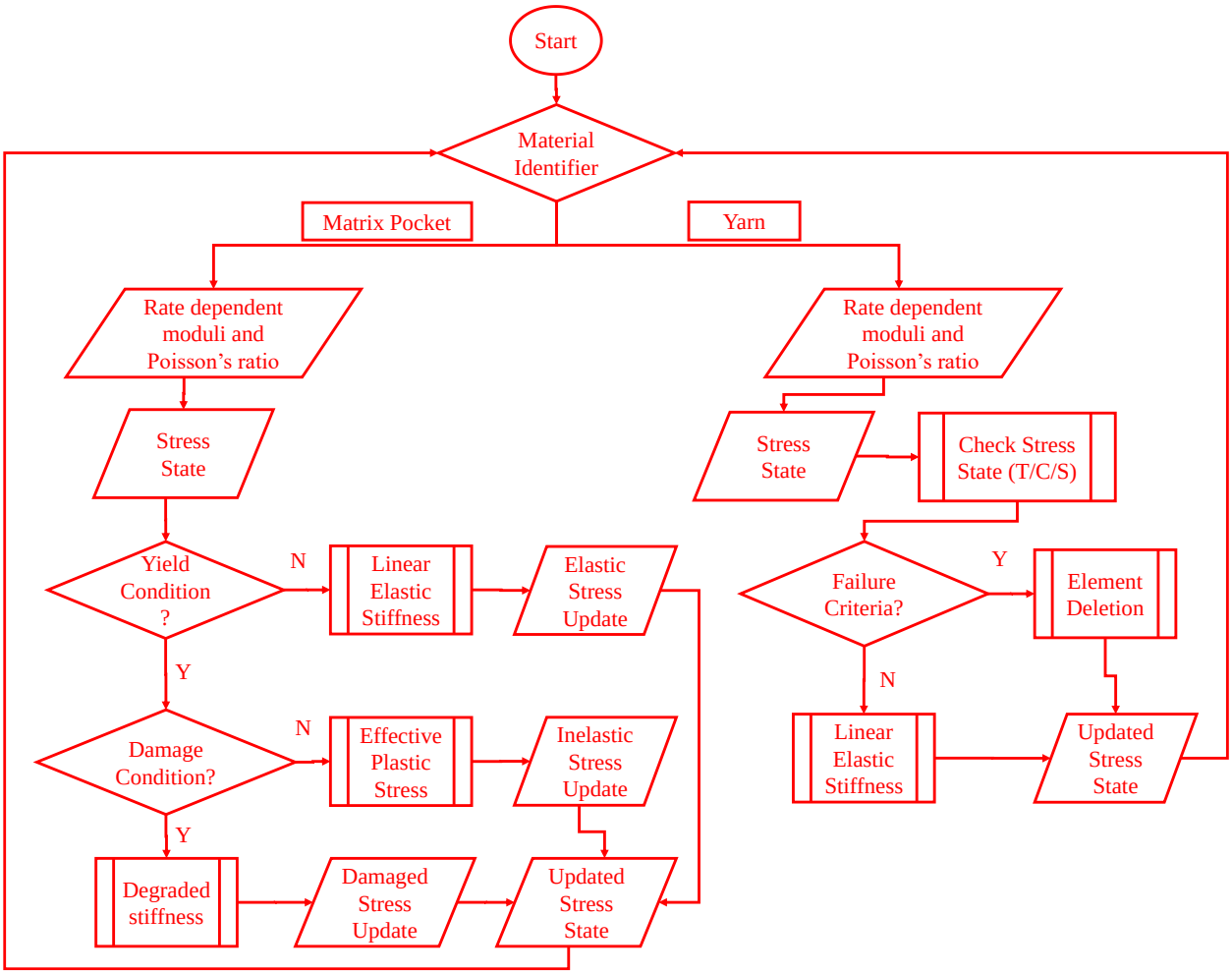

Figure A.2. Steps for meso-scale analysis

With the stress update algorithms (see Figure A.2), a homogenized response is evaluated by volume averaging. This serves as the inputs to the macro-scale. In the macro-scale analysis, the material models are implemented for the structure, Eulerian media (water, air), and explosive as Multi-Material ALE. The structural response is quantified in terms of the radial displacements (the center-point displacements are shown in Figure 10(b) in the main paper). The whole framework, micro-scale, meso-scale, and macro-scale models are integrated into a Python script that calls subroutines for each of the ABAQUS scripts and passes information to the next scale. The macro-scale analysis subroutine calls the LS-Dyna keyword file and runs the simulation in a double-precision solver. For double-precision solvers, output data can't be read by Python. So the output data are read using LS-PrePost software that enables only single output visualization and not batch mode. The central point displacements are exported as a time-history plot and post-processed.

B. Material Inputs

The section lists the material inputs at various scales for the fiber laminates. For the micro-scale analyses, the properties of matrices epoxy and vinyl ester; rate-dependent behavior of glass fiber and matrix; interfacial behavior are described in sub-section B-1. For mesoscale analyses, the homogenized properties from the micro-scale analyses are used to characterize the fiber tows and matrix pockets are assigned similar properties as in the micro-scale. The interfacial behavior of the fiber tow with matrix serves as input for the mesoscale simulations as explained in sub-section B-2. For the macro-scale laminate, the homogenized lamina properties as obtained from the mesoscale simulations are used. The adopted rate-dependent coating behavior for polyurea and rubber; the interlaminar characteristics of the laminate are provided in sub-section B-3.

B-1. Micro-scale Material Behavior

For the glass fiber-matrix unit cells, the matrix parameters are shown in Table B.1. These matrix properties are also used for matrix pockets in the mesoscale (see B-2). The input properties to the matrix are adopted for epoxy and vinyl ester from [1] and [2] respectively.

Table B.1. Matrix inputs for rate-dependent properties

Material constants	$D_0(s^{-1})$	N	$Z_0(MPa)$	$Z_1(MPa)$	q	α_0	α_1	$E_0(GPa)$	ν
Epoxy	10^6	0.93	400	750	90	0.6	0.13	2.84	0.38
Vinyl Ester	10^6	0.79	400	900	130	0.10	0.22	3.8	0.38

The rate-dependent behavior of the fiber and matrix are captured by $K_f(\dot{\varepsilon})$ and $K_m(\dot{\varepsilon})$ as shown in Equations B.1 and B.2 respectively. The K values are multiplied with quasi-static moduli and strengths to obtain the rate-dependent properties [3].

$$K_f(\dot{\varepsilon}) = 1 + 0.236(\dot{\varepsilon})^{0.2008} \quad \text{[B.1]}$$

$$K_m(\dot{\varepsilon}) = 1 + 1.1(\dot{\varepsilon})^{0.4478} \quad \text{[B.2]}$$

The CZM implemented in the interface between the glass fiber and matrix in micro-scale adopts properties as per Table B.2. The interface properties are obtained from [4] and [5]. The transverse loading strengths are based on interfacial features like friction factor adopted from [6–10].

Table B.2 Interface properties at micro-scale for loading directions between glass fiber and matrix

Load Case	Axial Load Case		Transverse Load Case	
Direction	Normal	Shear	Normal	Shear
Strength (MPa)	28	40	28	40
Critical Energy Release Rate (N/mm)	0.01	0.025	0.002	0.002
Friction Coefficient	-	-	0.4 (for compression)	

B-2. Meso-scale Material Behavior

The homogenized response of the micro-scale unit cells is used as material properties for the yarns. The properties of matrix pockets are shown in Table B.1. The glass fiber tow-matrix interface properties in the mesoscale are mentioned in Table B.3. The interfacial strength is adopted from [3] and the critical energy release rates are used from [11].

Table B.3 Glass fiber tow-matrix interface properties at mesoscale for plain weave unit cell

Direction	Normal	Shear
Strength (MPa)	27.6	10.3
Critical Energy Release Rate (J/mm^2)	0.28	1.45

B-3. Macro-scale Material Behavior

The lamina properties are obtained by homogenization of mesoscale woven unit cells. For failure analysis of the laminate, interlaminar characteristics are implemented in the macro-scale model. The interlaminar properties are provided in Table B.4. The properties are obtained from the literature [12,13].

Table B.4 Interlaminar properties for macro-scale laminated shell for macroscale UNDEX simulation

Direction	Normal	Shear
Strength (MPa)	35	68
Critical Energy Release Rate (N/mm)	1.21	4.55

For the coated configurations, the rate-dependent behaviors of the polymers are shown in Figure B.1. The data are adopted from [12,14] for polyurea and [15–18] for rubber.

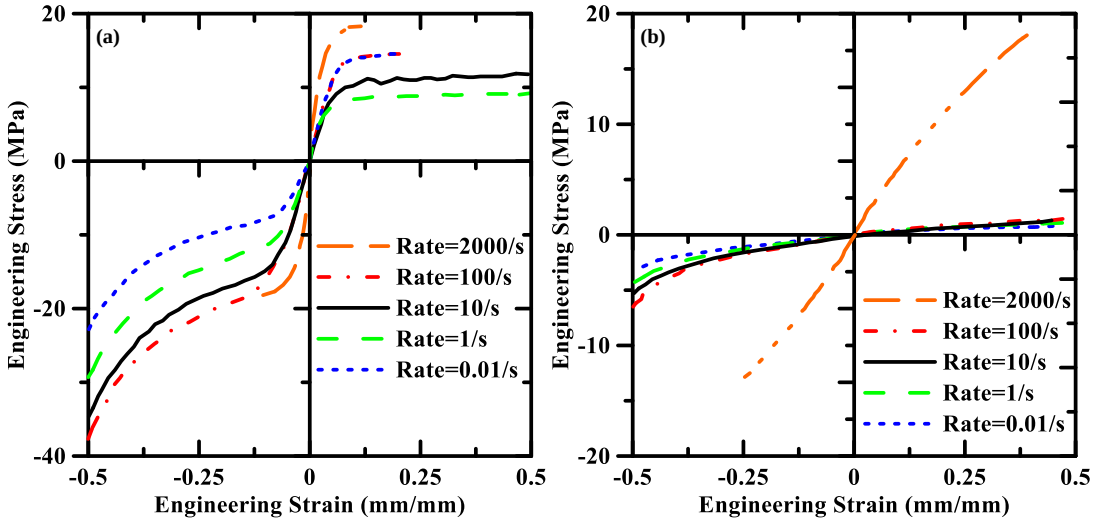

Figure B.1 Rate dependent load curves for (a) polyurea and (b) rubber used as coatings

C. Mesh Convergence

For the glass fiber-matrix micro-scale unit cell, an element size is chosen to adequately represent the geometry (upper limit being $0.8R^f$ where R^f is the radius of fiber). From Figure C.1(a), it can be observed that the optimum number of elements lies beyond 3x10^5. The chosen element size is $0.25R^f$ that generates 331836 elements. C3D10 elements are adopted for matrix and fiber while COH3D6 are adopted for interface in ABAQUS™. The mesh convergence for homogenized unit cell properties is shown in Figure C.1 (a). For the mesoscale weave unit cell, Figure C.1(b) shows the homogenized stress-strain behavior for the 2x2 weave unit cell with different number of elements (Nelem). The chosen element size for the mesh is governed by the thickness of the unit cell. The matrix pockets between adjacent tows and the regions of crossovers govern the minimum element size. The mesh convergence study (see Figure C.1(b)) shows the optimum element size as 0.022 mm that generates 2223642 elements. Further refinement increases the computational burden without significantly affecting the results.

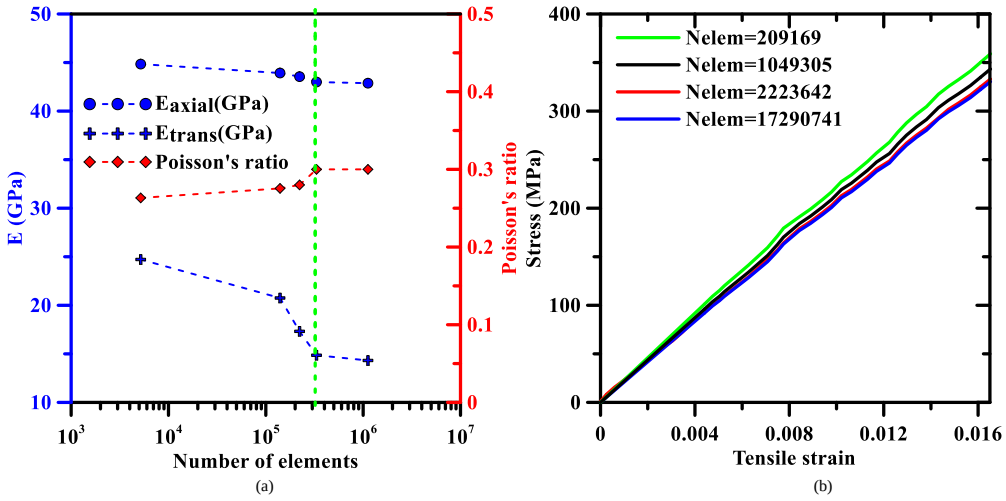

Figure C.1. (a) Homogenized properties for micro-scale unit cell with number of elements (b) Stress-strain response of mesoscale weave unit cell with varying number of elements (Nelem)

D. Through thickness behavior of weave

This Section elaborates the capability of the numerical framework to capture the through-thickness behavior of the woven unit cell. These capabilities are proven to be useful in thick laminates under high strain rates. The directional characteristics of the fiber yarns as obtained from the micro-scale unit cell homogenization enables the representation of the through-thickness behavior. Under through-thickness compression, a sample pressure contour is shown in Figure D.1. This serves as a demonstration of how the multiscale strategy developed in the study can be further used for macro-scale laminates where through-thickness considerations are necessary. However, the implementation of shell elements in the macro-scale for the laminate in the current study adopts in-plane properties along fill/warp and shear behavior, a strategy adopted after [13].

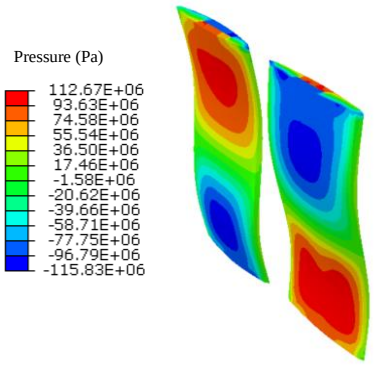

Figure D.1. Through thickness compression of weaves when compressed across the thickness of the plain weave unit cell (pressure contours on weft yarns)

E. DIC correlation with simulation

The correlation between the experimentally observed DIC and the contour displacements from the simulated model is added here to ensure the brevity of the manuscript. Although pressure-time histories and center-point displacements from the experimental observations and simulations are correlated in the manuscript, this supplementary section shows additional DIC plot [12] correlations that were evaluated to assess the prediction efficacy of the multiscale simulation strategy adopted in this study. Since there is a loss of correlation in the DIC data early on in the experiments for a standoff distance of 5.08cm, the correlation between the radial displacement fringes for the coated configuration is presented in Figure E.1 for a standoff distance of 2.54 cm. Even so, there is a loss of correlation for the thin coated cylinder. It is to be noted that the displacements are higher as the stand-off distance decreases. The DIC plots are presented on the left while the simulated contours are presented on the right for Figures E.1(a-d). Figures E.1 (a) and (c) correspond to a time of 2.5 ms while Figures E.1(b) and (d) correspond to a time of 2.75 ms. Figures E.1(a) and (b) show the radial displacement contours for the cylinder with a polyurea coating of 1.9 mm thickness. Figures E.1(c) and (d) show the radial displacement contours for the cylinder with a polyurea coating of 1.2 mm thickness. The simulated out-of-plane displacements are presented in a symmetrical color scale for an envelope over the time-steps in the transient analysis. The thicker coated configuration shows significantly higher resistance to deformation as enunciated from Figures E.1(b) and (d). Overall, a good correlation between simulated and experimental responses is obtained.

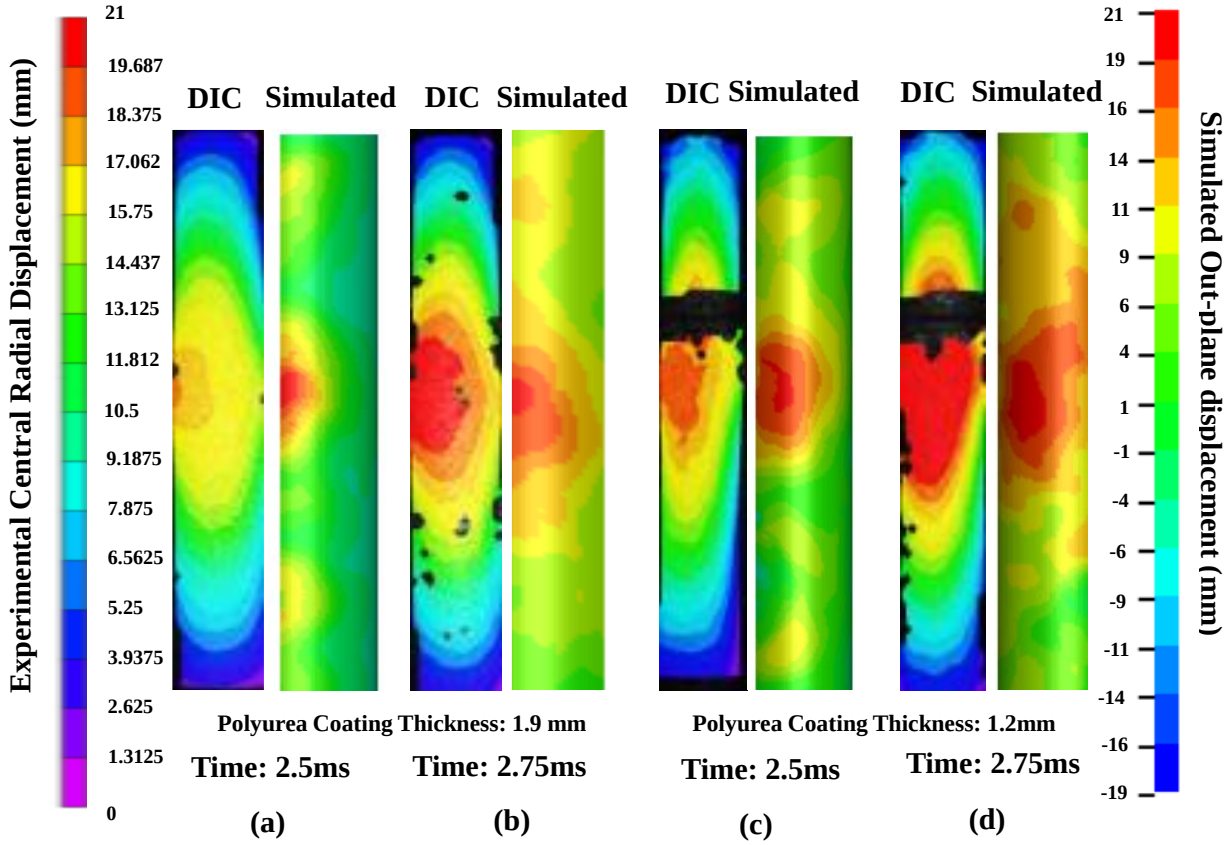

Figure E.1. DIC plots(left/experimental)[12] correlated with out-plane displacements from model(right/simulated) at different times for various coating thickness; (a) and (c) at 2.5ms; (b) and (d) at 2.75ms; (a) and (b) for 1.9 mm thick polyurea coating; (c) and (d) for 1.2 mm thick polyurea coating

More details about the displacement-time histories can be found in a previous publication [12]. In comparison to the previous study [12], the contribution to the macro-scale FE model lies in the adoption of a superior rate-dependent composite damage model implemented together with element deletion for stiffness reduction, *MAT_ENHANCED_COMPOSITE_DAMAGE. Figure 11 in the paper embodies the capability of the model to predict damage states as a superior damage prediction framework."

F. Optimized Neural Network

The raw data required to reproduce these findings are available to download from https://github.com/iamsumeru/Simulated-Dataset-UNDEX-Response-of-coated-composite-cylinders.git.

The optimized neural network that relates the input arguments (explosive energy, standoff distance, ratio of coating to wall thickness, material density) can be written as

$$Y = \boldsymbol{b}^{(3)} + \boldsymbol{w}^{(3)} \times f_{ReLU}\left(\boldsymbol{b}^{(2)} + \boldsymbol{w}^{(2)} \times f_{ReLU}\left(\boldsymbol{b}^{(1)} + \boldsymbol{w}^{(1)}\boldsymbol{X}\right)\right)$$

$\boldsymbol{w}^{(1)}$ = [3.5787672e-01, 3.6008824e-02, 2.2976210e+00, -1.5798155e+00,
 1.5274656e+00, 5.0010581e-02, -7.3463142e-01, -1.3835263e+00,
 4.4316146e-01, 1.2464844e+00, -4.1095728e-01, -9.8690581e-01,
-5.6640363e-01
-2.3504431e+00, 2.1494601e+00, 1.7816355e+00, 1.1326013e+00,
 1.3838967e+00, 2.8021148e-01, 3.1450310e-01, 1.2570410e+00,
 3.6005956e-01, -1.3037409e+00, -1.3392068e+00, 1.4575484e+00,
 6.2365200e-02
2.2388108e+00, -2.0640368e+00, 1.3141583e+00, -3.3248445e-01,
 7.8956820e-02, -4.2019886e-01, 1.9126658e+00, 8.4306550e-01,
-2.6119049e+00, -1.8483409e-01, -2.1315841e-01, -2.8235364e+00,
-1.4545805e+00
5.8360599e-02, 3.0060984e-02, 1.1726882e-03, -6.0556017e-02,
-7.5363752e-04, 1.0855848e+00, 3.0781070e-03, 6.1680269e-03,
 4.1532703e-02, -9.9239117e-03, -5.1922258e-02, 3.1101471e-03,
 9.7558223e-02]

$\boldsymbol{b}^{(1)}$ = [-1.0312814   0.02070769 -2.1925316   0.84171015 -1.0600013 -0.16831458
 0.07435013 1.1087983 -0.72331876 0.19386393 0.7867428 -1.4583977
 0.29987854]

$\boldsymbol{w}^{(2)}$ = [-1.5582073 , 0.8049131 , -2.4359272 , 1.4732991 , -1.6102514 ,
-3.659611 , 0.4683123 , -2.6663623 , -2.3785293 , -4.487542 ,
 0.8341938 , -0.39374933, -0.74603784
2.0212064 , 1.3901988 , 0.86965036, 3.2119243 , 1.7934995 ,
-0.59227616, 1.6411924 , 0.07799464, 1.7387044 , -4.4544077 ,
 0.4208878 , 2.7565653 , -3.2377603
-3.3260193 , -2.9723716 , -0.47826543, 1.1384056 , -3.4326136 ,
 2.2531905 , 0.758894 , 2.7423906 , 1.2606509 , 0.7341071 ,
 1.8947206 , -2.0428886 , 1.3605095
1.6001018 , -4.0344315 , 1.623524 , -2.1845698 , 1.5210493 ,
-0.924528 , -2.8549056 , 0.74948025, 1.5561496 , -1.3596898 ,
 1.5231717 , 1.5828581 , -1.555153
0.3006137 , 2.2685905 , 3.0475025 , -0.92962563, 0.13791381,
 4.217178 , -0.41863972, -2.7486753 , 2.6394656 , 1.347658 ,
 2.632649 , 0.45126584, -0.29171494
0.16707939, -1.0506485 , -0.06667978, -0.03328762, 0.15119368,
 0.33541265, -0.09828303, 0.19219379, 0.46525022, 0.14159796,
 0.6654007 , -0.48630556, -0.63730985
-2.2930896 , 0.2576932 , -2.5330253 , 0.0459212 , -3.041771 ,
 0.83769155, -1.999327 , -0.63000524, 2.180201 , -1.5909284 ,
-2.4055278 , 1.695237 , 1.9821686
-4.4937162 , 1.9342189 , 0.8559453 , -2.3611715 , -4.37544   ,
 0.8718658 , -1.4496855 , -0.15666166, 0.4472851 , 2.330417 ,
 0.32366925, -0.19334264, 0.41640702
-1.9495177 , 0.3331144 , -2.6125   , -0.12411975, -1.4943751 ,
-0.23878162, -0.8976723 , -0.5233301 , -2.4136305 , 3.0042138 ,
-3.274296 , -1.7755367 , 1.626026
1.0906812 , -1.3917978 , -1.1567523 , 0.09043925, 0.81629294,
 1.7077711 , 1.364858 , -3.052906 , -0.58544105, 1.9426073 ,
 1.2081361 , -3.4316168 , 1.7487019

-1.9661429 , 0.5497847 , -0.9199377 , 2.017678 , -1.7514105 ,
-0.7635476 , 2.322804 , 3.6814735 , 1.5454825 , 0.07804794,
0.18348181, 0.8037619 , 0.9643906
-2.3750856 , 1.6891469 , 1.1533927 , -1.6830953 , -2.4722536 ,
0.7159589 , 0.59009075, -1.1654416 , -0.5234647 , 1.6545366 ,
-0.31407148, -1.4966221 , 4.649927
0.8988839 , 2.6683805 , -0.2760152 , -2.1785848 , 0.35846132,
1.728206 , -1.6980715 , -0.73922986, 1.4484699 , -0.30558848,
1.246604 , 1.8819757 , -1.4734513]

$\boldsymbol{b}^{(2)}$ = [4.0573006 -4.1226506 1.7343427 0.01879389 4.6091623 0.15506247
3.0161827 0.7541007 -0.93635345 0.2152303 2.3054814 0.92982155
0.2381337]

$\boldsymbol{w}^{(3)}$ = [2.5009315
0.5418429
-0.55236614
0.3994296
-2.4338653
-0.70676655
-0.55822915
-0.6701195
0.698528
0.8026265
0.5727067
-0.5429504
-0.47530845]

$\boldsymbol{b}^{(3)}$ = 1.7527281

The input arguments followed a standardized scaling written as:

$$\boldsymbol{X} = \left\{\frac{x_i - \mu_i}{\sigma_i}\right\}, i = 1,2,3,4$$

μ = [0.86076262, 8.60799622, 1.53657007, 2.7494229]

σ= [0.3547, 5.0268, 0.7064, 0.2072]

where x is the input arguments, μ is the mean value and σ standard deviation. f_{ReLU} is the Rectified Linear Unit activation function written as:

$$f_{ReLU}(x) = max(0, x)$$

REFERENCES

[1] Goldberg R, Roberts G, Gilat A. Implementation of an Associative Flow Rule Including Hydrostatic Stress Effects Into the High Strain Rate Deformation Analysis of Polymer Matrix Composites. Journal of Aerospace Engineering 2003;18. https://doi.org/10.1061/(ASCE)0893-1321(2005)18:1(18).

[2] Shams A, Panteghini A, Bardella L, Porfiri M. A micromechanical model to study failure of polymer-glass syntactic foams at high strain rates. Computational Materials Science 2017;135:189–204. https://doi.org/10.1016/j.commatsci.2017.04.007.

[3] Ma D, Manes A, Amico SC, Giglio M. Ballistic strain-rate-dependent material modelling of glass-fibre woven composite based on the prediction of a meso-heterogeneous approach. Composite Structures 2019;216:187–200. https://doi.org/10.1016/j.compstruct.2019.02.102.

[4] Ogihara S, Koyanagi J. Investigation of combined stress state failure criterion for glass fiber/epoxy interface by the cruciform specimen method. Composites Science and Technology 2010;70:143–50. https://doi.org/10.1016/j.compscitech.2009.10.002.

[5] Zhang H, Ericson ML, Varna J, Berglund LA. Transverse single-fibre test for interfacial debonding in composites: 1. Experimental observations. Composites Part A: Applied Science and Manufacturing 1997;28:309–15. https://doi.org/10.1016/S1359-835X(96)00123-6.

[6] Romanowicz M. A numerical approach for predicting the failure locus of fiber reinforced composites under combined transverse compression and axial tension. Computational Materials Science 2012;51:7–12. https://doi.org/10.1016/j.commatsci.2011.07.039.

[7] Romanowicz M. Determination of the first ply failure load for a cross ply laminate subjected to uniaxial tension through computational micromechanics. International Journal of Solids and Structures 2014;51:2549–56. https://doi.org/10.1016/j.ijsolstr.2014.03.030.

[8] Akash Sharma, , Subbareddy Daggumati. Computational micromechanical modeling of transverse tensile damage behavior in unidirectional glass fiber-reinforced plastic composite plies: Ductile versus brittle fracture mechanics approach -. International Journal of Damage Mechanics 2020.

[9] Sharma A, Daggumati S, Gupta A, Van Paepegem W. On the prediction of the bi-axial failure envelope of a UD CFRP composite lamina using computational micromechanics: Effect of microscale parameters on macroscale stress–strain behavior. Composite Structures 2020;251:112605. https://doi.org/10.1016/j.compstruct.2020.112605.

[10] Alireza Khademi, Mahmood M Shokrieh, Shahram Etemad Haghighi. A novel model to predict the stiffness and strength of unidirectional glass/epoxy composites at different strain rates -. Journal of Composite Materials 2020.

[11] Nayak S, Das S. Strain sensing efficiency of hierarchical nano-engineered smart twill-weave composites: Evaluations using multiscale numerical simulations. Composite Structures 2021;255:112905. https://doi.org/10.1016/j.compstruct.2020.112905.

[12] Gauch E, LeBlanc J, Shukla A. Near field underwater explosion response of polyurea coated composite cylinders. Composite Structures 2018;202:836–52. https://doi.org/10.1016/j.compstruct.2018.04.048.

[13] Schwab M, Pettermann HE. Modelling and simulation of damage and failure in large composite components subjected to impact loads. Composite Structures 2016;158:208–16. https://doi.org/10.1016/j.compstruct.2016.09.041.

[14] LeBlanc J, Shukla A. Response of polyurea-coated flat composite plates to underwater explosive loading. Journal of Composite Materials 2015;49:965–80. https://doi.org/10.1177/0021998314528263.

[15] Kolling S, Bois PAD, Benson DJ, Feng WW. A tabulated formulation of hyperelasticity with rate effects and damage. Comput Mech 2007;40:885–99. https://doi.org/10.1007/s00466-006-0150-x.

[16] Kolling S. A Simplified Rubber Model with Damage. . LS 2005:10.

[17] Kumar D, Sarangi S. Data on the viscoelastic behavior of neoprene rubber. Data in Brief 2018;21. https://doi.org/10.1016/j.dib.2018.10.081.

[18] Trivedi AR, Siviour CR. A Simple Rate–Temperature Dependent Hyperelastic Model Applied to Neoprene Rubber. J Dynamic Behavior Mater 2020;6:336–47. https://doi.org/10.1007/s40870-020-00252-w.